Article | Received 12 May 2026; Revised 15 May 2025; Accepted 15 May 2025; Published 22 June 2026
https://doi.org/10.55092/sc20260012

Experimental investigation on cohesion-friction mechanical properties for early-age concrete

Dechun Lu[1], Zhiyuan Guo[1], Tao Cai[1], Guosheng Wang[1,*], Zhiwei Gao[2] and Xiuli Du[1]

[1] Key Laboratory of Urban Security and Disaster Engineering of Ministry of Education, Beijing University of Technology, Beijing 100124, China
[2] Glasgow Computational Engineering Centre (GCEC), James Watt School of Engineering, University of Glasgow, Glasgow G12 8QQ, UK

* Correspondence author; E-mail: wangguosheng@bjut.edu.cn.

Highlights:

- The validity of an innovative experimental method for investigating the cohesion-friction properties of early-age concrete has been verified.
- The decoupling of cohesion strength and friction strength in early-age concrete has been achieved.
- The deformation mechanisms underlying the cohesion and friction properties in early-age concrete have been revealed.

Abstract: As a core material in modern construction, the early-age properties of concrete have a decisive impact on the safety and durability of civil engineering structures. However, systematic research on the mechanical properties of early-age concrete remains limited, particularly regarding the combined influence of cohesive and frictional properties on the material's macroscopic mechanical behavior, which has not been thoroughly explored. To address this gap, this paper employs a decoupling method for testing the cohesion-friction mechanical properties of concrete, as proposed in previous work. This method successfully separates the cohesive and frictional properties of early-age concrete, validating its applicability under early-age conditions and obtaining typical failure modes following material performance degradation. Furthermore, by analyzing the evolution patterns of cohesive and frictional properties during deformation and strength development, the synergistic mechanism of cohesion-friction mechanical properties in early-age concrete was revealed. The results indicate that the responses of cohesive and frictional properties to hydrostatic pressure in early-age concrete exhibit significant differences. The reduction in macroscopic shear strength and stiffness is fundamentally attributed to the irreversible dissipation of cohesive strength. Ultimately, the mechanical behavior of early-age concrete gradually approaches that of granular materials without cohesion.

Keywords: early-age concrete; triaxial test; cohesion-friction properties; deformation behavior; strength evolution

1. Introduction

Enhancing urban resilience, especially the ability to cope with natural disasters such as earthquakes and extreme environments, is one of the core objectives of modern urban development [1]. The achievement of this goal deeply relies on the precise understanding of the basic mechanical behaviors of its constituent materials. Concrete, as the most widely used material in urban construction, directly determines the performance and durability of engineering structures through its mechanical properties. Existing research has shown that concrete is a friction-type material with cementitious properties, where cement gel provides cohesion, and the interlocking effect between aggregates exhibits the frictional properties of geotechnical materials [2–4].

Given the composition and formation properties of concrete materials, their macroscopic mechanical properties exhibit significant cohesion-friction properties. Based on this understanding, Wang *et al.* decomposed the macroscopic shear strength of concrete into cohesive strength and frictional strength [4]. The cohesive strength is independent of hydrostatic pressure and exhibits mechanical properties similar to metallic materials, while the frictional strength increases with the increase of hydrostatic pressure. Nevertheless, prevailing research paradigms generally do not differentiate between cohesive and frictional properties. Instead, concrete strength is conventionally classified according to test configuration—namely, uniaxial compressive/tensile strength [5–7], biaxial strength [8], and triaxial strength [9]—without quantitatively assessing the relative contributions of cohesive *versus* frictional strength components. In fact, the proportion of cohesive and frictional strength exerted in different types of macroscopic shear strength of concrete varies greatly. For example, in uniaxial tensile strength [10], the cohesive strength plays a larger role, while in conventional triaxial compressive strength under high confining pressure, the frictional strength dominates. By elucidating the mobilization mechanisms of cohesive and frictional properties, concrete strength under varying loading paths can be directly characterized via the evolution of their respective strengths. This understanding provides a theoretical foundation for fundamentally solving the path dependence of concrete strength and simplifying the establishing process of concrete strength theory and constitutive models.

As the primary material for modern architecture, the early performance of concrete plays a crucial role in determining the durability and safety of civil engineering structures [11–13]. Current research on the crack propagation, deformation and strength properties of concrete materials mainly focuses on specimens under standard curing age. In contrast, systematic studies on the mechanical properties of early-age concrete are still insufficient, especially regarding the influence mechanism of cohesion and friction properties on the macroscopic mechanical behavior of the material. There is no clear and in-depth understanding yet in this regard [14]. Compared with standard curing age concrete with relatively stable and dense microstructure, the hydration reaction of early-age concrete has not fully occurred, its microstructure is not fully developed, and the cohesion strength has not been fully formed. Therefore, it is particularly sensitive to the damage mechanisms such as micro-crack initiation and propagation [14–17]. This inherent characteristic highlights the role of frictional resistance in the overall mechanical response and also leads to the fact that early-age concrete is more prone to deplete its cohesion properties during the mechanical response process, thus providing favorable research conditions for the separation and systematic analysis of the cohesive-frictional coupling mechanical behavior. In addition, conducting research on the cohesion-friction mechanical properties of early-age concrete can provide key parameters

for structural safety assessment, and is directly related to post-disaster emergency repair and rapid construction projects such as tunnel lining, foundation pit support, and slope anchoring [18,19].

To investigate the cohesive-frictional mechanical properties of early-age concrete and the respective mechanisms of their effects, this study selected three different strength grades of early-age concrete and conducted systematic triaxial compression tests under four confining pressure levels. Based on the systematic analysis of the test results, this study clarified the macroscopic mechanical behavior of early-age concrete, revealed the intrinsic relationship between its deformation and strength related to cohesion and friction, and thereby clarified the mechanisms of the cohesion-friction mechanical properties of early-age concrete of different strength grades under different confining pressure conditions.

2. Experimental materials and program

To conduct the aforementioned research, concrete specimens meeting the experimental requirements were prepared using raw materials including ordinary Portland cement, coarse aggregate, and fine aggregate. It should be noted that the early age of concrete typically refers to multiple stages ranging from initial setting to 28 days of curing. This study focuses on the 3-day period, which is critical for early-stage hydration reactions and strength development; the term ‘early age’ as used in this paper specifically refers to 3 days under standard curing conditions. This study primarily employed conventional triaxial compression tests under four distinct confining pressure conditions to comprehensively evaluate the mechanical properties of the early-age concrete specimens.

2.1. Cement and aggregates

The cementitious material selected for this study is Type II ordinary Portland cement PO42.5R, which meets the technical requirements of the national standard GB175-2007. This cement comprises Portland cement clinker, appropriate blended materials, and gypsum. It exhibits high strength, significant hydration heat, low drying shrinkage, and excellent abrasion resistance, though its corrosion resistance is relatively poor. Its detailed chemical composition and component ratios are shown in Figure 1a.

During the preparation of concrete specimens, both coarse and fine aggregates were selected. The coarse aggregate consisted of medium sand with a fineness modulus of 2.86 and crushed stone with particle sizes ranging from 5 to 16 millimeters. The gradation curve for the coarse aggregate is shown in Figure 1c. River sand was selected as the fine aggregate, and its gradation curve, obtained through sieve analysis, is shown in Figure 1d.

2.2. Specimens preparation

Concrete specimens were prepared in the concrete laboratory of the west campus at Beijing University of Technology. Specimen preparation followed the procedures specified in the standard test methods for physical and mechanical properties of concrete. Mix proportions for concrete of different strength grades are detailed in Table 1. The dimensions of concrete specimens produced for this study are shown in Figure 1b. Concrete mixing was performed using a small single-shaft concrete mixer. Fresh water used for testing was sourced from the Beijing municipal waterworks.

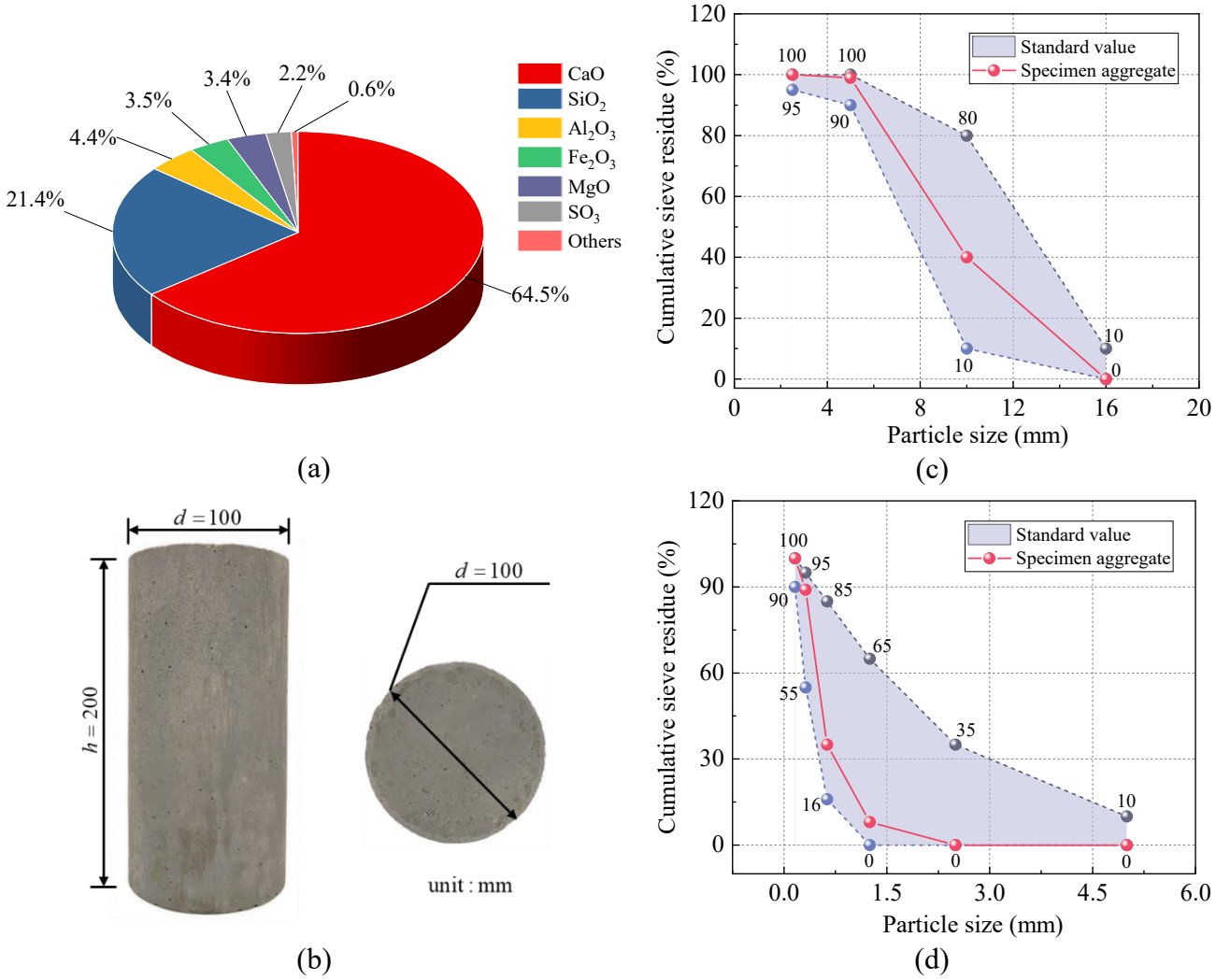

Figure 1. Concrete specimen: **(a)** Chemical composition and proportion of cement; **(b)** Size type of concrete specimen; **(c)** Coarse aggregate; **(d)** Fine aggregate.

Table 1. Mix proportion design of concrete.

Strength grade	Coarse aggregate (kg/m^3)	Fine aggregate (kg/m^3)	Cement (kg/m^3)	Water (kg/m^3)
C30	1178.88	634.78	317.00	190.00
C40	1196.31	553.96	388.00	190.00
C50	1195.66	476.59	475.00	190.00

The concrete mixing method employs the cement-coated sand and gravel technique. After mixing is complete, the fluid concrete is discharged from the drum and all mixed concrete is placed into the corresponding molds within 30 minutes. The mixed concrete is placed into the molds in two layers, with each layer thoroughly compacted using a vibrating table until no visible air bubbles emerge from the concrete surface. Upon concrete placement, the specimens were set at ambient temperature on a level surface for 24 hours, during which the molds were covered with transparent PVC sheets to minimize moisture loss. After this initial curing, the specimens were demolded and transferred to a standard curing chamber maintained at 20 ± 2 °C with relative humidity exceeding 95% for 3 days.

2.3. Experimental apparatus

This study performed conventional triaxial tests using the high-temperature and high-pressure comprehensive rock testing system. The system consists primarily of a high-pressure triaxial cell, a confining pressure intensifier, and a digital signal conditioning and control unit. During testing, silicone oil was injected into the triaxial cell. The confining pressure was then applied by a computer-controlled actuator that compressed the silicone oil, with a maximum achievable confining pressure of 140 MPa. After the confining pressure stabilized at the target value, axial load was imposed on the specimen via a strain-controlled axial actuator. The axial loading capacity of the system is 1500 kN. In the experiment, a circumferential LVDT sensor and two axial LVDT sensors were used to measure circumferential strain ε_3 and axial strain ε_1 respectively; the volumetric strain ε_v is given by $(\varepsilon_1 + 2\varepsilon_3)$. Strain was determined from the ratio of the deformation during loading to the original gauge length of the specimen. The LVDT sensors have a measurement range of ± 6 mm and an accuracy of 1e−3 mm.

2.4. Experimental program

This study utilizes a testing approach previously proposed by the author to isolate the cohesive and frictional components of concrete behavior [16]. By conducting multiple complete triaxial compression tests on the same concrete specimen, the stress–strain response obtained during the first loading reflects the combined contribution of both cohesive and frictional mechanisms. This initial loading induces complete failure of the specimen, thereby exhausting its cohesive capacity to the greatest extent possible. The same specimen is then reloaded under identical initial conditions, yielding a stress–strain curve governed almost exclusively by frictional properties. The triaxial tests were conducted under drained conditions, and there was no influence of pore water pressure. Since the cohesive contribution is largely eliminated after the first loading, the subsequent test results predominantly capture the frictional response. A comparison of the two loading test results enables the decoupling of the cohesive and frictional properties of early-age concrete. This method offers a new perspective for separately obtaining the independent deformation and strength evolution patterns of the cohesive phase (*i.e.*, cementitious matrix) and the friction phase *(i.e.,* aggregates) under complex stress conditions, thereby aiding in further elucidating the macroscopic performance mechanisms underlying the cohesive-frictional behavior of concrete. To prevent the heat-shrink tubing, which serves as an insulator, from rupturing due to excessive circumferential strain, stop loading once the axial strain reaches 2%; keep the axial actuator stationary, remove the specimen after releasing the confining pressure. To minimize the impact of human error on the test data, reposition the LVDT sensor on the test bench and immediately begin the second loading.

The sample numbers, quantities, and corresponding confining pressures are listed in Table 2. In the numbers, C30, C40, and C50 represent the concrete strength grades; “F” indicates the first loading test, “S” indicates the second loading test under the same conditions; “P” and the subsequent numbers represent the confining pressure values of the triaxial tests; i = 1, 2, 3 are the parallel test sequence numbers. The tests use four confining pressures of 0, 3 MPa, 6 MPa, and 9 MPa. All tests use axial strain control, with a loading rate of 0.001%/s and a data acquisition interval of 2 seconds [20,21].

Table 2. Experimental scheme for cohesion-friction properties.

Strength grade	Specimen number			Quantity	Confining pressure (MPa)
	C30FP0-*i*	C40FP0-*i*	C50FP0-*i*		0
C30	C30FP3-*i*	C40FP3-*i*	C50FP3-*i*		3
	C30FP6-*i*	C40FP6-*i*	C50FP6-*i*		6
C40	C30FP9-*i*	C40FP9-*i*	C50FP9-*i*	3	9
	C30SP3-*i*	C40SP3-*i*	C50SP3-*i*		3
C50	C30SP6-*i*	C40SP6-*i*	C50SP6-*i*		6
	C30SP9-*i*	C40SP9-*i*	C50SP9-*i*		9

3. Experimental results and discussion

This section employs the experimental protocol described in Section 2.4, utilizing the GCTS RTR1500 High-Temperature High-Pressure Rock Testing System to conduct uniaxial and triaxial compression tests on the mechanical properties of C30, C40, and C50 concrete. Based on the test results, an in-depth analysis of the cohesion-friction properties of concrete materials under complex stress environments is presented.

3.1. Macroscopic mechanical properties of early-age concrete

3.1.1. Failure modes

In conventional triaxial compression tests, the circumferential constraint provided by confining pressure significantly alters the friction mechanical response of concrete materials. As shown in Figure 2, for all concrete specimens cured for 3 days, the failure patterns under different confining pressures after two loading exhibited the following properties: All specimens displayed macroscopic cracks traversing the diagonal. This failure mode, after excluding external factors such as silicone oil, showed well-developed cracking in the specimens. Under uniaxial compression, specimens primarily exhibited splitting failure, characterized by dominant longitudinal cracks on the surface with low microcrack development [22]. As initial hydrostatic pressure increases, the failure mechanism of concrete gradually shifts toward shear failure. Specifically, high confining pressure suppresses the propagation of vertically oriented cracks dominated by tensile stress [23–26]. This induces slip and shear deformation between particles within the material, generating microcracks at original defects such as interfaces between aggregates and cement matrix or within material voids. These microcracks propagate slowly along planes of maximum shear stress, significantly enhancing shear strength and ductile deformation capacity. This mechanical strengthening effect enables concrete to withstand greater shear deformation during stress redistribution without tensile failure, ultimately exhibiting typical shear failure properties.

Additionally, the reinforcing effect of confining pressure activates the material's friction properties, manifested as a significant increase in microcrack density on the specimen surface accompanied by volumetric expansion [23]. Comparative analysis indicates that the splitting-shear failure mode of C40 and C50 concrete exhibits similar mechanical behavior to C30 concrete. As concrete strength grades increase, the stress levels it can withstand under identical initial hydrostatic pressure also rise, enabling greater dissipation of external load energy. This energy dissipation process manifests at the material level as increased microcracking, a phenomenon that becomes increasingly pronounced with higher hydrostatic pressure.

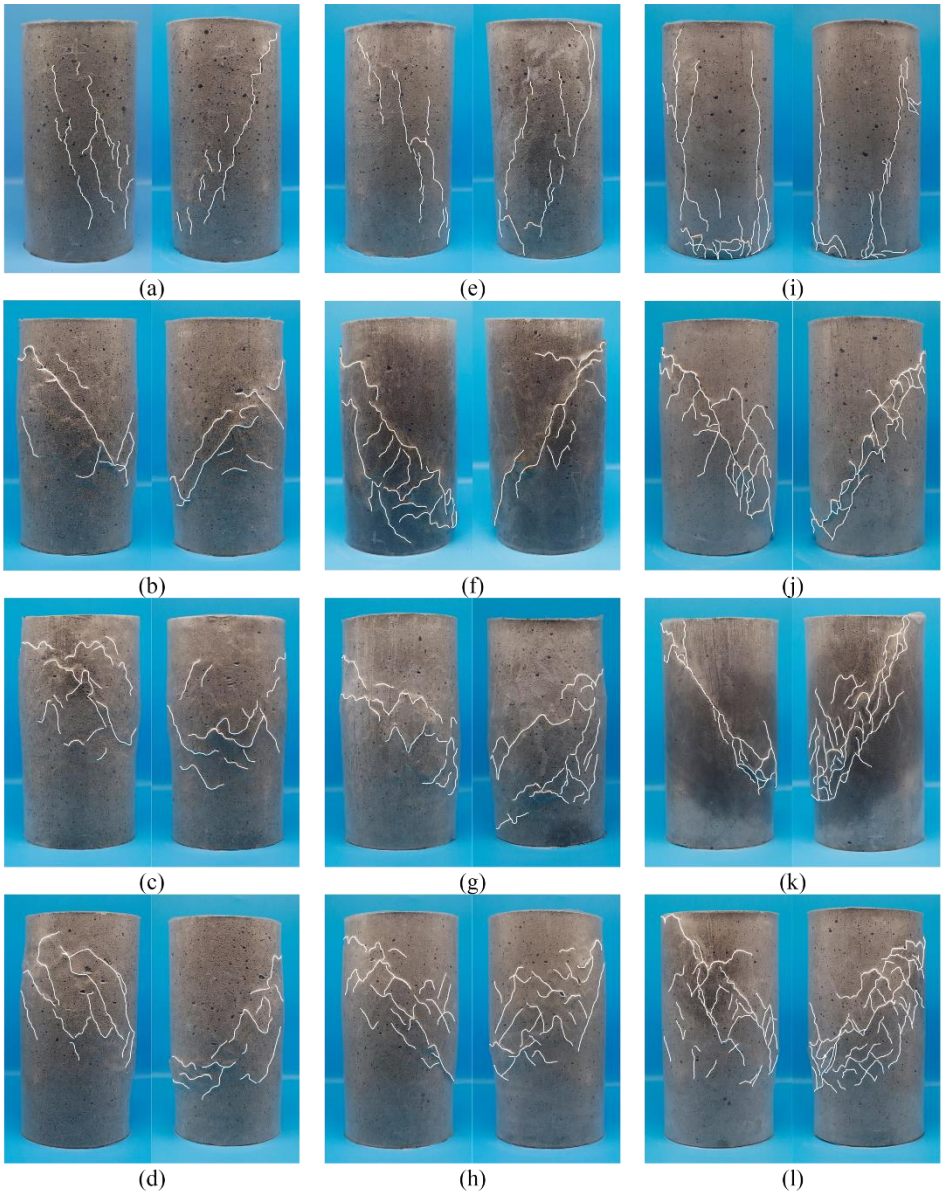

Figure 2. Failure modes of concrete specimens: **(a)** C30FP0; **(b)** C30SP3; **(c)** C30SP6; **(d)** C30SP9; **(e)** C40FP0; **(f)** C40SP3; **(g)** C40SP6; **(h)** C40SP9; **(i)** C50FP0; **(j)** C50SP3; **(k)** C50SP6; **(l)** C50SP9.

3.1.2. Deformation properties of early-age concrete

The stress-strain curves from conventional triaxial compression tests on three different concrete strength grades under four distinct initial hydrostatic pressures are shown in Figure 3. For each strength grade, three parallel test sets were conducted under varying confining pressures to minimize random errors caused by incidental factors, thereby enhancing the precision and reliability of the test results. Average stress-strain curves under different initial hydrostatic pressure conditions were calculated through linear interpolation, with specific results shown in Figure 3. The three parallel curves in this paper show little difference in the post-peak softening region, and their failure strains are very close. Based on the common strain range, we performed linear interpolation across the entire segment using small strain increments of 0.02%, then calculated the mean value at each point to obtain the average curve. The consistency between the deformation patterns revealed by the averaged data and those from the original test results further validates the reliability of the testing process and outcomes.

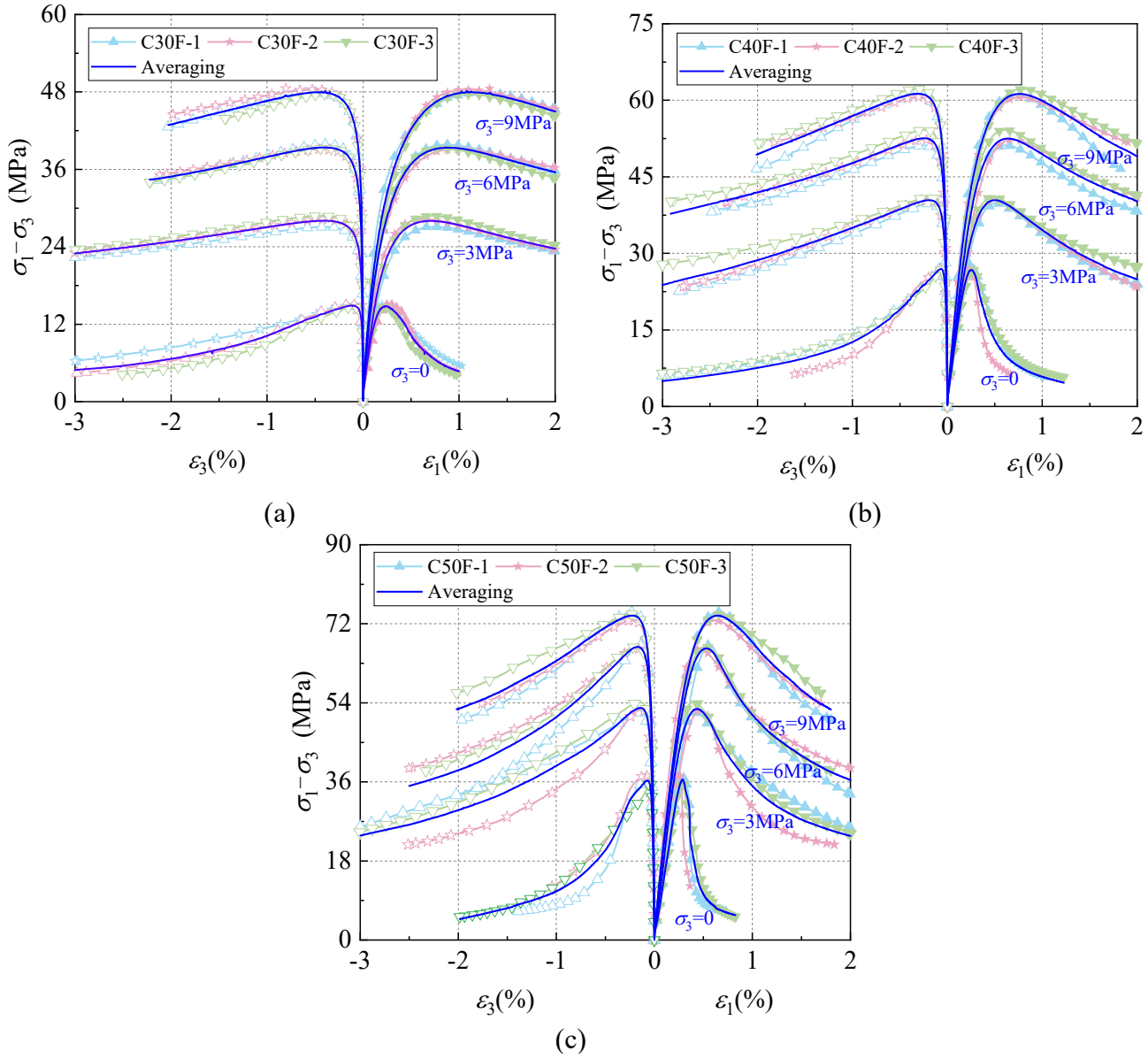

Figure 3. Average stress-strain curves of concrete specimens: **(a)** C30F; **(b)** C40F; **(c)** C50F.

The deformation data for C30 concrete in Figure 3 indicate that under uniaxial loading condition, the absence of confining pressure allows microcracks to rapidly form and propagate both internally and externally within the specimen. The external load-bearing capacity decreases sharply, manifesting as pronounced strain softening behavior on the stress-strain curve after reaching peak stress. It is evident that in conventional triaxial compression tests, the confining pressure provides hoop restraint that effectively limits crack propagation both inside and outside the concrete specimen. During deformation, even if strain softening occurs after the specimen reaches peak stress, it is no longer as pronounced compared to uniaxial compression test results. Simultaneously, as confining pressure increases, the peak stress of concrete also rises, with corresponding axial and hoop strains gradually increasing. The post-peak region of the deformation curve becomes progressively flatter, resulting in a more rounded curve profile. Figure 3b,c demonstrates that C40 and C50 concrete exhibit deformation patterns similar to C30 concrete. Comparing the deformation curves of the three strength grades under identical confining pressure reveals that as concrete strength increases, the peak stress rises while strain softening becomes more pronounced.

3.1.3. Strength properties of early-age concrete

Comparing the macroscopic shear strength of the three concrete grades under different confining pressures reveals that the strengthening effect of confining pressure on shear strength gradually diminishes as confining pressure increases. Compared to C30 concrete, cohesion strength contributes a larger proportion to the macroscopic shear strength of C40 and C50 concrete, while confining pressure has a limited effect on cohesion strength. Consequently, the enhancement effect of confining pressure on the macroscopic shear strength of C40 and C50 concrete is far less pronounced than that on C30 concrete, resulting in a correspondingly smaller increase in peak stress.

The cohesive strength and friction strength of concrete materials can be clearly demonstrated through strength properties on the meridian plane. Within this plane, the generalized shear stress q and hydrostatic pressure p correspond to the vertical and horizontal coordinates, respectively, with their specific expressions as follows:

$$p = \frac{\sigma_1 + \sigma_2 + \sigma_3}{3} \tag{1}$$

$$q = \frac{1}{\sqrt{2}}\sqrt{(\sigma_1 - \sigma_2)^2 + (\sigma_2 - \sigma_3)^2 + (\sigma_3 - \sigma_1)^2} \tag{2}$$

Here, σ_1, σ_2, and σ_3 represent the major, intermediate, and minor principal stresses in the principal stress space. In conventional triaxial compression tests, $\sigma_2 = \sigma_3$. By substituting the principal stresses into Equations (1) and (2), the hydrostatic pressure p and generalized shear stress q at the strength point under different confining pressures were obtained. By performing linear fitting on the hydrostatic pressure p and generalized shear stress q at the strength points, the strength curve on the meridian plane was obtained, as shown in Figure 4.

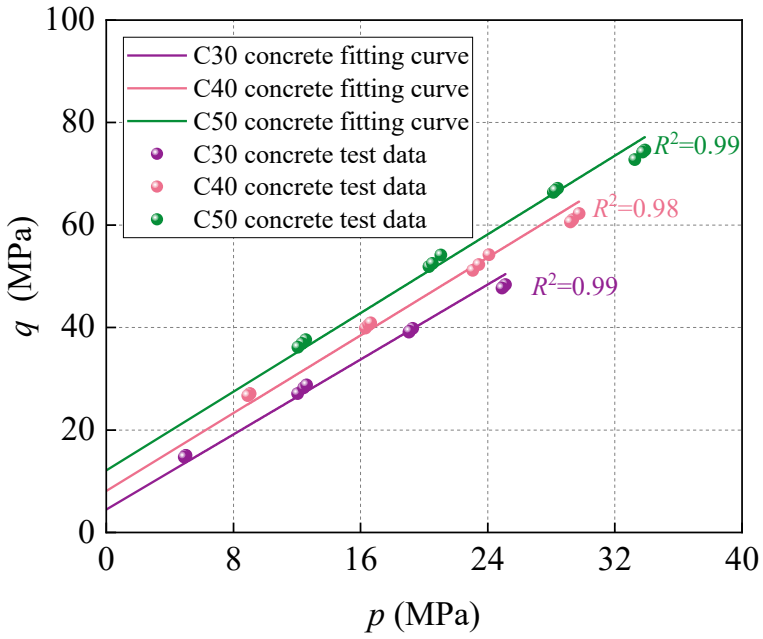

Figure 4. Strength properties of specimens on the meridional plane during initial loading.

The high fitting correlation coefficients R^2 indicate that the strength data fits well. The intersection of the strength curve with the vertical axis represents cohesion q_c. For concrete materials, cohesion q_c is positively correlated with cohesive strength σ_0, while the slope corresponds to the tangent value of the

internal friction angle [3]. Based on the linear fitting results, cohesion q_c and internal friction angle φ were calculated for concrete of various strength grades: q_c = 4.50 MPa for C30 concrete, φ = 61.33°; for C40 concrete, q_c = 8.07 MPa, φ = 62.24°; for C50 concrete, q_c = 12.10 MPa, φ = 62.50°. Comparative calculations indicate that as concrete strength grades increase, cohesion rises and cohesive strength also grows; the internal friction angle of early-age concrete specimens exhibits minimal variation. The fundamental reason for this parameter response difference lies in the insufficient development of the matrix bonding strength in early-age concrete materials, resulting in a lower stress tolerance level. At lower stress levels, the friction strength differences between concrete of varying strength grades are relatively small. Similar friction angles indicate that the strength differences between concrete grades primarily stem from variations in cohesive strength.

3.2. Cohesion-friction properties of early-age concrete

3.2.1. Deformation properties

Since this study utilized concrete specimens cured for only 3 days under standard curing conditions, the current specimens' macroscopic shear strength could not reach the material's design strength. Simultaneously, the cohesive strength of the concrete significantly decreased after the initial loading, rendering the specimens incapable of sustaining axial loads under unconfined conditions. Therefore, the study employed the testing method described in Section 2.4 to analyze the cohesion-friction properties of the concrete material exclusively under conventional triaxial compression test conditions with confining pressures of 3 MPa, 6 MPa, and 9 MPa. Figure 5 presents the stress-strain curves of early-age concrete specimens from the three strength grades during the second loading process under different confining pressures. Results indicate that for C30, C40, and C50 concrete, the peak stress (*i.e.*, frictional strength) of the stress-strain curve gradually increases with rising confining pressure. Under identical confining pressure conditions, the peak stress values and corresponding axial and hoop strains of different strength concrete grades were relatively close. This indicates that the macroscopic shear strength differences among concrete grades under the same confining pressure are primarily governed by cohesion strength.

Additionally, strain softening was still observed in the deformation curves of some specimens, indicating that the cohesive strength of the specimens had not been fully exhausted. However, compared to the first loading deformation results of concrete specimens in Figure 3, post-peak strain softening was not pronounced, exhibiting deformation properties similar to pure friction geomaterials like sandy soils. Comparing Figure 5b,c to Figure 5a reveals that C40 and C50 concrete exhibit friction deformation properties similar to C30 concrete. Furthermore, the friction strength differences among concrete of varying strength grades under identical confining pressure are relatively minor. The fundamental mechanism lies in the fact that, under identical confinement conditions, the friction strength component within the macroscopic shear strength of concrete of different strength grades remains relatively stable. Conversely, the cohesion strength component demonstrates a pronounced gradient strengthening effect as the material strength grade increases.

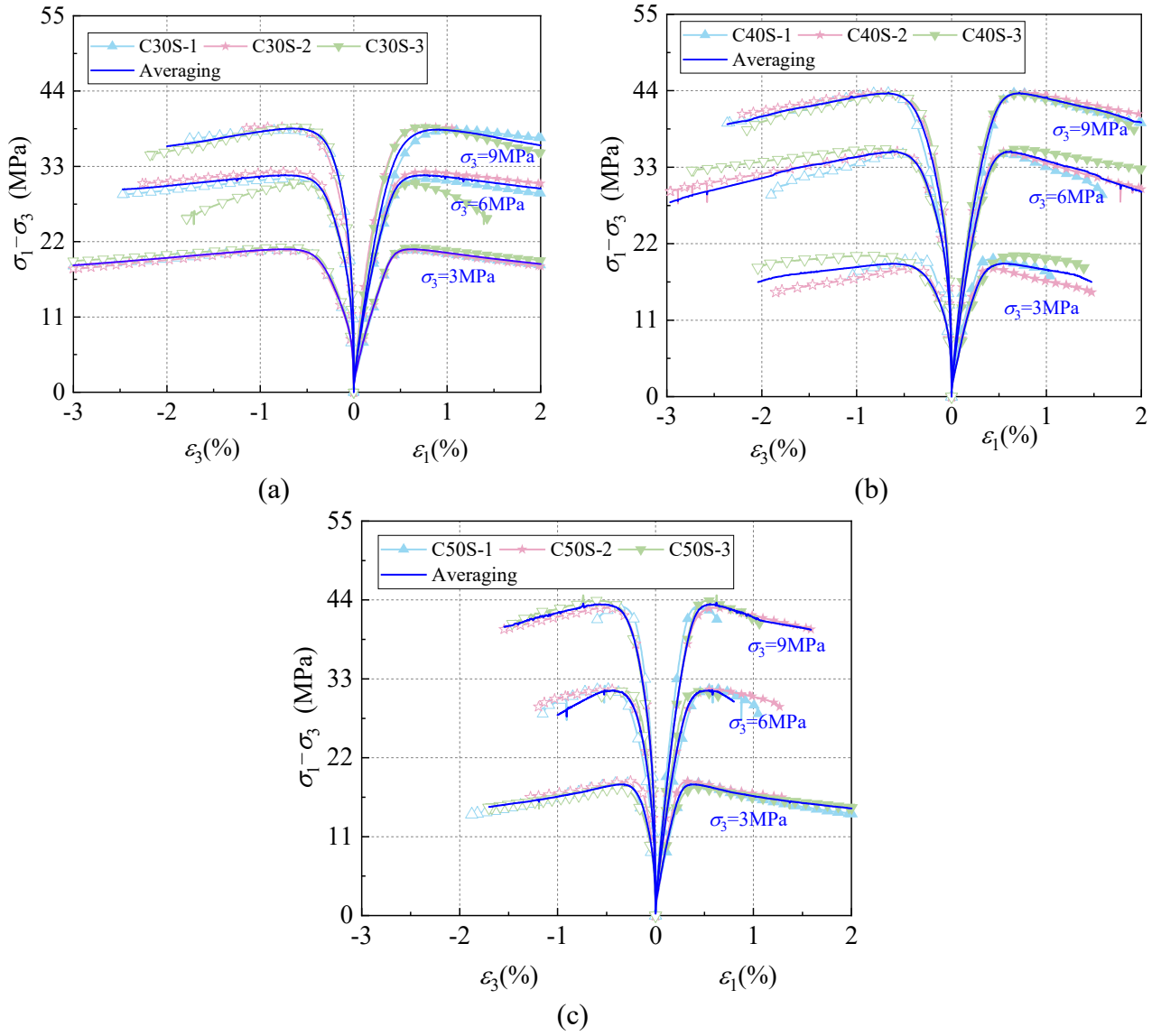

Figure 5. Average stress-strain curves of concrete specimens: **(a)** C30S; **(b)** C40S; **(c)** C50S.

By comparing the stress-strain curves obtained from two loading tests conducted under identical confining pressure conditions on the same specimen, the cohesion-friction coupling mechanism of early-age concrete materials can be effectively revealed. Figure 6 displays the deformation curves from the first and second loading tests under different confining pressures for three strength grades concrete cured for 3 days. The comparison reveals that the three strength grades exhibit similar deformation patterns: the deformation curve of the first loading test shows significant strain softening compared to the second loading test. As concrete strength grades increase, the post-peak segment of the first loading deformation curve becomes steeper under identical confining pressure, indicating more pronounced strain softening. Combining friction deformation test results reveals that friction strength is approximately equal across different strength grades under the same confining pressure. However, higher concrete strength grades exhibit greater macroscopic shear strength under identical confining pressure, consequently yielding higher cohesion strength. Although the first loading may not completely exhaust the cohesive strength of the concrete material, its residual value at the end of loading becomes negligible compared to the initial state.

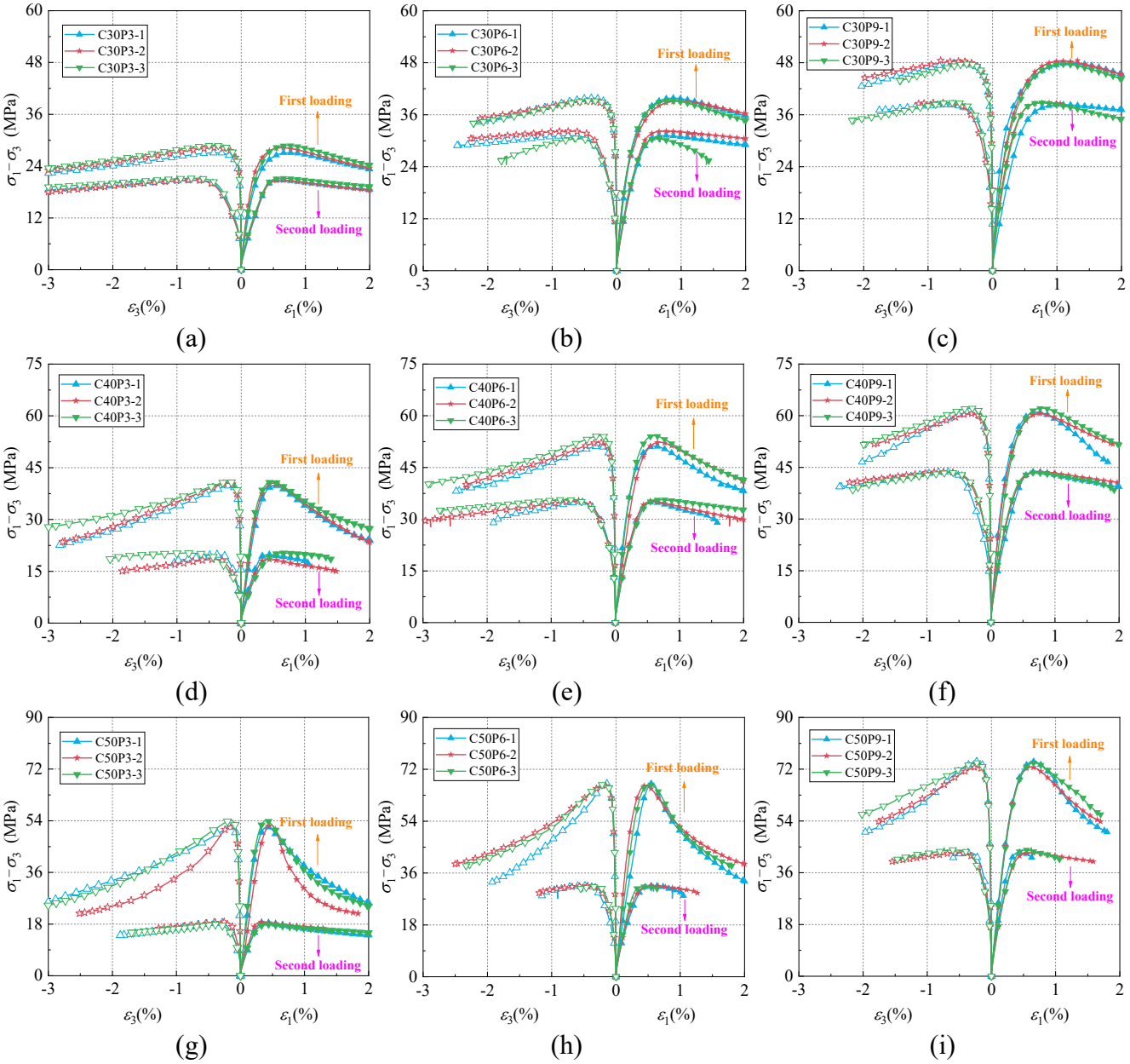

Figure 6. Comparison of stress-strain curves of two triaxial compression tests on the same concrete specimen: **(a)** C30P3; **(b)** C30P6; **(c)** C30P9; **(d)** C40P3; **(e)** C40P6; **(f)** C40P9; **(g)** C50P3; (h) C50P6; **(i)** C50P9.

According to the method for determining the static compressive modulus of elasticity of concrete specified in ASTM C469-02 standard test method for static modulus of elasticity and Poisson's ratio of concrete in compression, the modulus of elasticity reflected in the deformation curves of concrete specimens of different strength grades under varying confining pressures was extracted from Figure 6. The results are shown in Figure 7. The data in the figure represent the average values from three parallel tests conducted under identical conditions. As shown in the figure, the cohesive strength of the concrete specimens continuously deteriorates with loading. Consequently, the elastic modulus measured in the first loading test is consistently higher than that obtained in the friction loading test (second loading), indicating degradation in both the strength and stiffness of the concrete material. This deformation characteristic further validates the damage mechanism revealed by Wang *et al.* [27], where both cohesion strength and stiffness of concrete materials degrade during loading. Additionally, for concrete

of the same strength grade, increasing initial confining pressure enhances the elastic modulus exhibited during deformation. Under identical confining pressure, the elastic modulus values for concrete of different strength grades in both loading tests increase with higher strength grades.

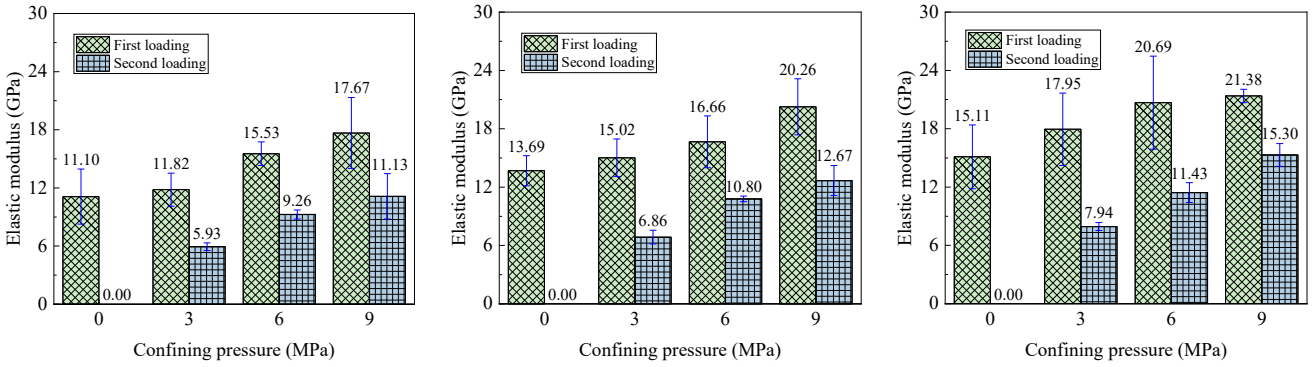

(a) (b) (c)

Figure 7. Comparison of elastic modulus of two loaded concrete specimens: **(a)** C30 concrete; **(b)** C40 concrete; **(c)** C50 concrete.

Based on the failure mode and deformation characteristics of the specimens, it can be observed that during the initial stage of shear loading, the concrete first bears hydrostatic pressure, generating an initial friction component. At this stage, the cohesion between the coarse aggregate and the mortar matrix, as well as at their interfaces, provides the entire shear resistance; deformation is entirely contributed by the cohesion mechanism. Internal damage is minimal, and the overall stiffness is high, resulting in near-linear elastic deformation. As the load continues to increase and the shear strength is reached, the specimen undergoes plastic deformation, and microcracks gradually initiate internally, causing the cohesive properties to gradually dissipate. With further loading, the microcracks propagate and induce plastic slip at the crack interfaces, causing the concrete to exhibit nonlinear elastoplastic damage and deformation behavior. The initiation of new cracks, combined with the propagation and penetration of existing cracks, leads to a continuous decline in overall stiffness and cohesive strength, resulting in significant strain softening. Once cohesive properties are completely lost, the entire external load is transferred to the friction units. Since the initial loading had already fully utilized the cohesive properties, the test results from the second loading exhibit significant friction characteristics [16].

3.2.2. Dilatancy properties

The dilatancy properties of concrete at different strength grades under varying confining pressures during two loading tests are shown in Figure 8. The results indicate that the volume change of concrete under different stress states can be divided into two stages: the volume contraction stage (volume strain $\varepsilon_v > 0$) and the volume dilation stage (volume strain $\varepsilon_v < 0$). During the initial loading phase, positive volume strain indicates the specimen is in a state of contraction. As the load increases, the volume strain gradually rises to a peak, then decreases to zero and turns negative, signifying the specimen has entered the volume dilation phase. Comparing the results of the two loading tests reveals that the maximum volume strain for all three concrete strength grades was greater during the first loading than during the second. Additionally, higher confining pressure resulted in larger maximum volume strain values for specimens of the same strength grade. This phenomenon can be explained from the perspective of

internal material evolution: During the initial phase of the first loading, the concrete contained initial voids formed by incomplete hydration or inadequate compaction [7]. As the load increased, the specimen gradually compacted, reducing its overall volume and exhibiting shear contraction behavior. Higher confining pressure results in greater compaction of the specimen during the volumetric contraction phase. Since the first loading has already closed a significant number of initial voids, and further compression of these voids is difficult under the same initial hydrostatic pressure during subsequent loading, the volumetric change during the second loading is significantly reduced.

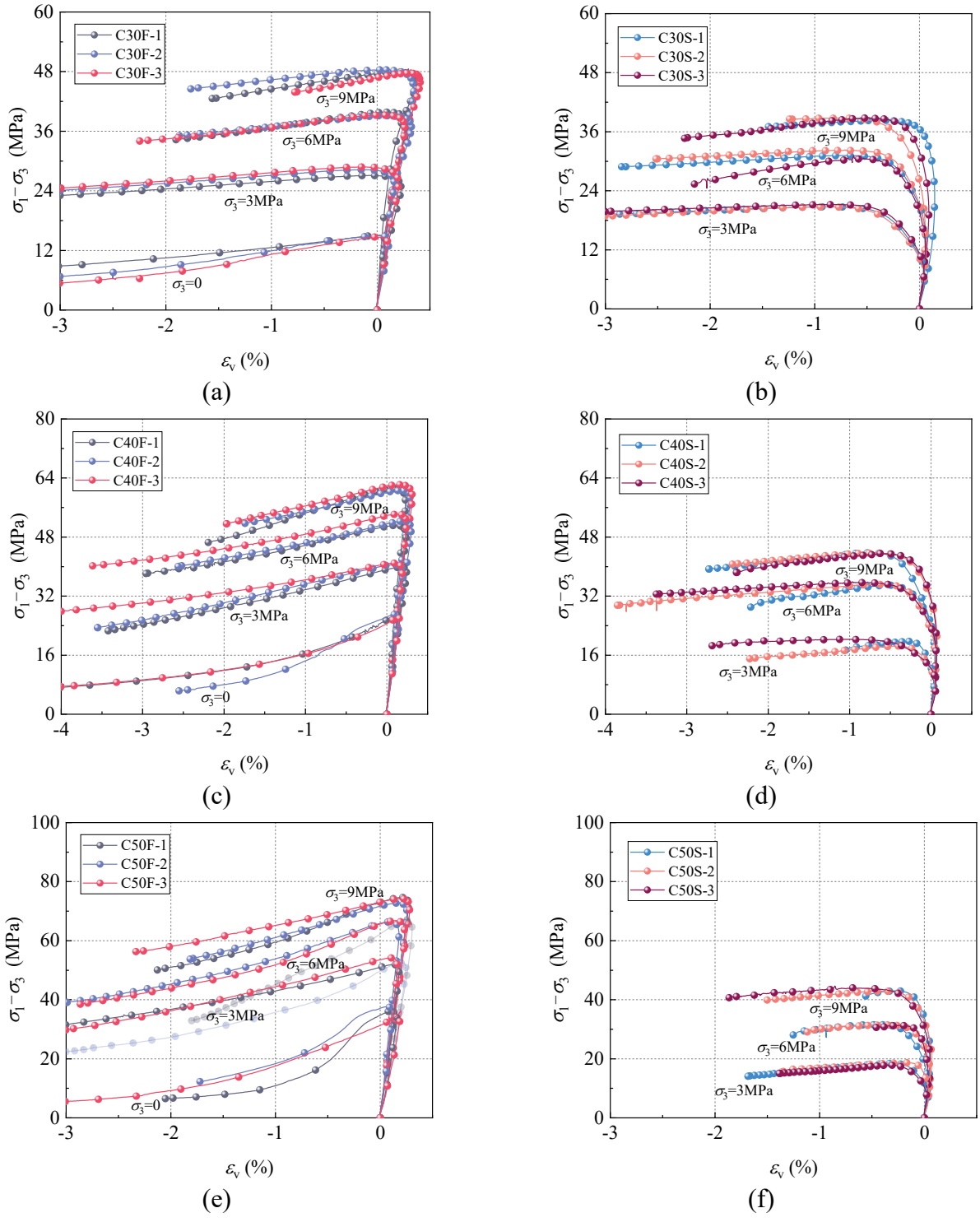

Figure 8. Volume strain-stress curves of concrete specimens: **(a)** C30F; **(b)** C30S; **(c)** C40F; **(d)** C40S; **(e)** C50F; **(f)** C50S.

3.2.3. Strength properties

Based on the hydrostatic pressure p and generalized shear stress q at the strength points for concrete of the same strength grade under different loading conditions, linear fitting was applied to plot the strength curves on the meridian plane for concrete of different strength grades, as shown in Figure 9. The correlation coefficients of the linear fitting functions for the test data of C30, C40, and C50 concrete at the 3-day curing age all exceeded 0.996. The strength curves on the meridian plane indicate that during the second loading test: C30 concrete exhibited residual cohesion and internal friction angle of 0.40 MPa and 61.32°, respectively; C40 concrete showed residual cohesion and internal friction angle of 0.30 MPa and 62.24°, respectively; while C50 concrete exhibited residual cohesion and internal friction angle of 0 and 62.22°, respectively. Comparative analysis reveals minimal differences in residual cohesion and internal friction angle among the three concrete grades. Compared to the first loading test results, residual cohesion is nearly negligible. This indicates that shear strength during the second loading process is primarily provided by friction strength. Compared to the first loading test, the linear relationship between specimen strength and load significantly strengthened during the second loading test, as evidenced by the correlation coefficient for linear fitting increasing to 0.996. This phenomenon primarily arises because the second loading test predominantly exploits the material's friction properties, and pure friction properties exhibit a more linear relationship with changes in stress state.

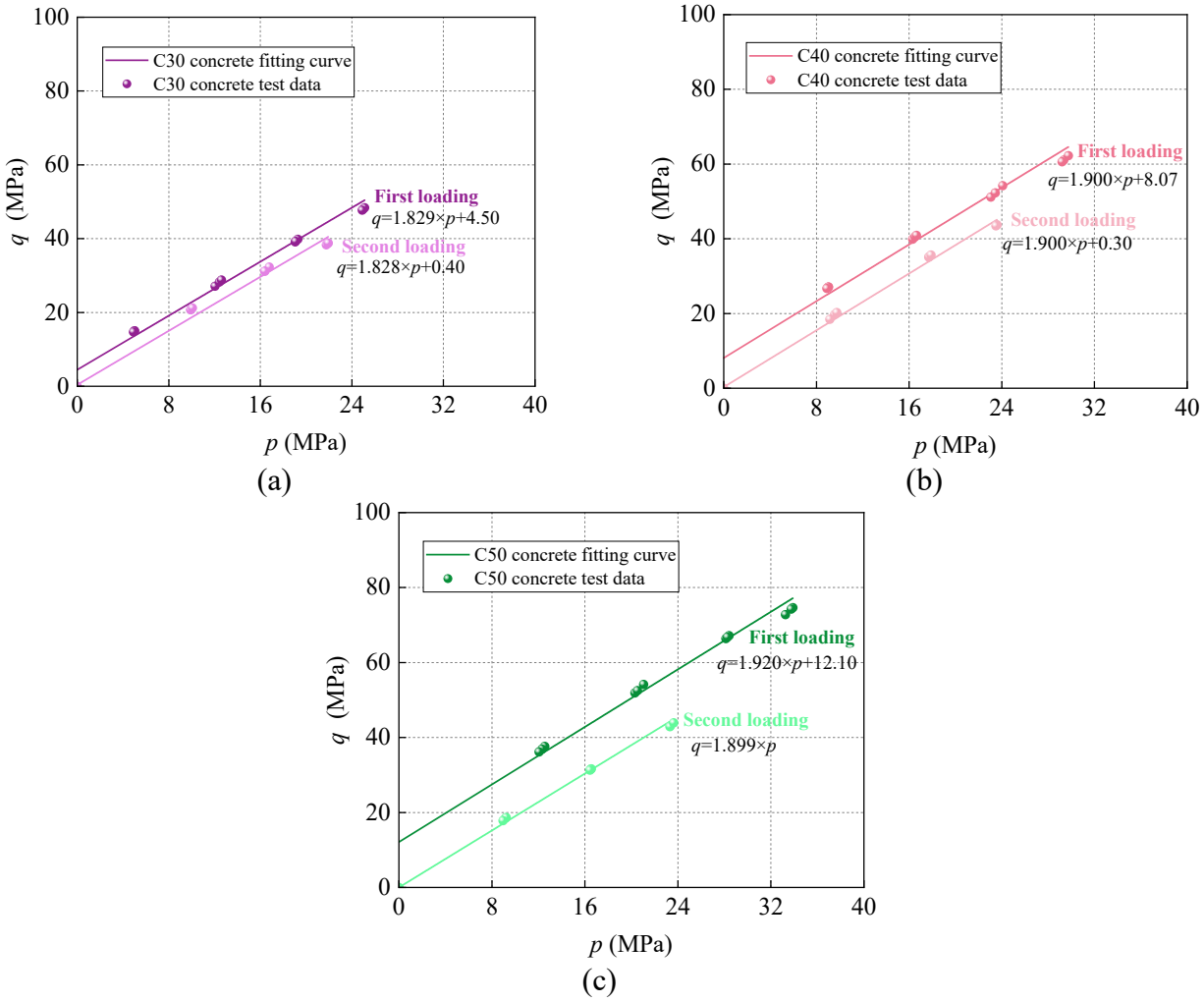

Figure 9. Comparison of strength curves of concrete loaded twice on the meridian plane: **(a)** C30 concrete; **(b)** C40 concrete; **(c)** C50 concrete.

Comparing the strength curves of three concrete specimens with different strength grades and a curing age of 3 days under two loading on the meridian surface, as shown in Figure 9. The two strength curves are nearly parallel, validating Wang *et al.*'s view that cohesion strength remains unaffected by hydrostatic pressure, while friction strength is significantly influenced by hydrostatic pressure [4].

During the first loading, the cohesive strength of concrete exhibits non-uniform variation, while the fracture of coarse aggregates and mortar occurs randomly [28–30]. Together, these factors result in a stress-strain curve displaying pronounced nonlinear properties. In contrast, during the second loading, the cohesive strength is largely depleted, and the fracture of coarse aggregates and mortar at lower stress levels is significantly reduced. Consequently, the strength curve exhibits a stronger linear trend. These phenomena indicate that concrete, as a cohesive-frictional material, derives its shear strength from both cohesion and friction, while its deformation behavior encompasses both solid deformation and inter-particle frictional deformation. During loading, the progressive loss of cohesive properties suggests that damage primarily affects the material's cohesive properties; as damage intensifies, the role of frictional behavior becomes increasingly prominent. When the concrete is completely destroyed in its limit state, its cohesive strength is completely lost. At this time, the shear strength depends entirely on the friction strength.

4. Conclusion

This study focuses on early-age concrete as the experimental subject. A test method capable of evaluating the cohesion-friction mechanical properties of the material was employed, and triaxial compression tests were conducted using a high-temperature and high-pressure rock testing system. This method effectively separates the cohesive and frictional properties of concrete, revealing their respective evolution laws during deformation and strength development, thereby elucidating the combined action process of cohesion and friction mechanisms in early-age concrete. The relatively low cohesive strength of early-age concrete provides favorable experimental conditions for investigating cohesion-friction mechanical properties. The main conclusions are as follows:

(1) The feasibility of the author's previously proposed test method for analyzing the cohesion-friction mechanical properties of early-age concrete is verified. The cohesive and frictional properties of early-age concrete were decoupled experimentally. A two-stage loading procedure was adopted to obtain both the macroscopic mechanical behavior reflecting the combined effect of cohesion and friction and the mechanical response reflecting only the frictional properties.

(2) Under the same confining pressure, the difference in macroscopic shear strength among early-age concretes of different strength grades is primarily determined by their cohesive strength, while their frictional strength remains largely consistent. Confining pressure influences the shear performance of concrete by modulating the frictional strength, within the confining pressure range of this experiment, the cohesion strength exhibits relatively low sensitivity to confining pressure.

(3) During the loading process, the cohesive properties of early-age concrete are continuously consumed, and the frictional properties gradually become prominent. The reduction in macroscopic shear strength and stiffness fundamentally originates from the irreversible dissipation of cohesive strength. Under the sustained action of external loads, material damage is mainly manifested as the degradation of cohesive properties, accompanied by a progressively enhanced frictional response. Ultimately, the mechanical behavior of early-age concrete approaches that of a cohesionless soil.

It should be noted that both loading test methods employed in this study involve the coupling of cohesion and friction properties; however, the cohesive behavior exhibited by the same specimen during the second loading cycle is virtually negligible. Furthermore, microcracks and structural damage generated during the initial loading stage alter the interlocking structure between aggregates to some extent. This study will be further refined in the future through numerical simulation.

Data availability statement

No supplementary or additional data were generated in this study. All data generated during this study were included in this published article.

Declaration of generative AI and AI-assisted technologies

During the preparation of this manuscript, the authors used generative AI tools only to improve language and readability. Specifically, the authors used DeepSeek for language polishing only in limited sections. The authors take full responsibility for the content of the manuscript.

Acknowledgments

Support for this study is provided by the National Natural Science Foundation of China (Grant Nos. U25B20214, 52438005 and 52378471) and the Natural Science Foundation of Beijing, China (Grant No. 8252002).

Authors' contribution

Dechun Lu: conceptualization, writing—review and editing, methodology, resources and funding acquisition; Zhiyuan Guo: investigation, writing—original draft, formal analysis and visualization; Tao Cai: investigation, writing—original draft, formal analysis, data curation and visualization; Guosheng Wang: writing—review and editing, methodology, conceptualization, resources and funding acquisition; Zhiwei Gao: supervision and project administration; Xiuli Du: resources and project administration. All authors have read and agreed to the published version of the manuscript.

Conflicts of interest

Xiuli Du holds the position of Editor-in-chief for *Smart Construction* and has not peer reviewed or made any editorial decisions for this paper.

References

[1] Hu J, Wen W, Zhai C, Pei S. A comprehensive review of resilience of urban metro systems: a perspective from earthquake engineering. *Tunn. Undergr. Space Technol.* 2024, 152:105920.

[2] Wang G, Lu D, Du X, Zhou X, Cao S. A true 3D frictional hardening elastoplastic constitutive model of concrete based on a unified hardening/softening function. *J. Mech. Phys. Solids.* 2018, 119:250–273.

[3] Huang D, Nie X, Liu T, Fan J. Quantitative analysis on cohesion, friction, and dowel action on concrete interfaces: experimental and theoretical approaches. *Eng. Struct.* 2025, 338:120624.

[4] Fu Z, Zhu H, Yu Z, Liu P, Guo Z, *et al.* Influence of various factors on the bonding properties of interface between LUHPC and NC based on cohesion and friction coefficient. *J. Eng. Mech*. 2026, 86:111446.
[5] Ren Z, Li D. Uniaxial compressive behavior study of normal-strength concrete using waste steel slag aggregate through laboratory tests and numerical simulation. *J. Build. Eng.* 2024, 85:108720.
[6] Li H, Pel L, You Z, Smeulders D. Stress-dependent instantaneous cohesion and friction angle for the Mohr–Coulomb criterion. *Int. J. Mech. Sci.* 2024, 283:109652.
[7] Shi D, Chen X, Ning Y, Ji T. Deformation responses and strength criteria of different shotcrete-rock composites under triaxial cyclic compression. *Constr. Build. Mater.* 2023, 374:130935.
[8] Bosbach S, Hegger J, Classen M. Compression softening of textile CFRP reinforced concrete (CRC): biaxial testing of cracked CRC panels and derivation of constitutive laws. *Constr. Build. Mater.* 2024, 444:137739.
[9] Zeng J, Hu X, Sun H, Liu Y, Chen W, *et al.* Triaxial compressive behavior of 3D printed PE fiber-reinforced ultra-high performance concrete. *Cem. Concr. Compos.* 2025, 155:105816.
[10] Wu Z, Zhang J, Yu H, Wu Q, Da B. Computer-aided investigation of the tensile behavior of concrete: relationship between direct and splitting tensile strength. *Structures* 2023, 55:453–467.
[11] Ding J, Wang X, Waisman H, Geng Z, Wu Z. Unified chemo-thermo-hygro-mechanical framework for early-age concrete. *Int. J. Mech. Sci.* 2026, 312:111162.
[12] Ding J, Wang X, Ren X, Waisman H, Wu Z. A thermodynamically consistent and strongly coupled chemo–thermo–hygral framework for early-age concrete. *Eur. J. Mech. A/Solids* 2026, 117:105992.
[13] Li K, Wu Z, Zheng X, Wang Y, Zhang Y. Comparative analysis of different machine learning models for prediction of compressive strength of early-age frozen concrete. *Cold Reg. Sci. Technol.* 2026, 224:104808.
[14] Fan X, Liu S, Wei D, Ge F. Fracture characteristics and damage evolution of early-age concrete under cyclic loading: insights from AE and DIC techniques. *Eng. Fract. Mech.* 2025, 330:111685.
[15] Cao L, Cao P, Wang Z, Tan Z, Shi F, *et al.* Application of SCMs and seawater to cement-bonded calcareous sand: macro performance, micro mechanism, and strength prediction. *Constr. Build. Mater.* 2024, 419:135560.
[16] Wang G, Cai T, Lu D, Ma C, Meng F, *et al.* Experimental study on cohesion-friction mechanical properties for concrete. *Constr. Build. Mater.* 2024, 449:138421.
[17] Zhang P, Kai M, Dai J. A chemo-thermo-viscoelastic model for early-age concrete behaviors. *Int. J. Mech. Sci.* 2025, 296:110304.
[18] Sciumè G, Benboudjema F, De Sa C, Pesavento F, Berthaud Y, *et al.* A multiphysics model for concrete at early age applied to repairs problems. *Eng. Struct.* 2013, 57:374–387.
[19] Chai L, Yue Z, Guo L, Huang Y, Chen B. Mechanical constitutive behavior and microstructure evolution of high ductility concrete rapid repair material at different curing ages. *Constr. Build. Mater.* 2025, 458:139600.
[20] Zhang Y, Yang F, Zhao C, You H, Zhen J. Experimental and numerical study of failure mechanisms of ultra-hard granite rock bridges under high-pressure triaxial compression: implications for natural fault segment linkage. *Theor. Appl. Fract. Mech.* 2026, 146:105756.

[21] Kou Y, Jiang Z, Li J, Song W, Tang B, *et al.* Study on the mechanical properties and macro–micro scale damage characteristics of rock-like-backfill composite structure under true triaxial loading. *Eng. Fail. Anal.* 2026, 193:110907.

[22] Wang Y, Wang Y, Zhao Y, Li G, Lyu Y, *et al.* Experimental study on ultra-high performance concrete under triaxial compression. *Constr. Build. Mater.* 2020, 263:120225.

[23] Jiang X, Li Q, Yin X, Xu S. Investigation on triaxial compressive mechanical properties of ultra high toughness cementitious composites with high strain capacity. *Cem. Concr. Res.* 2023, 170:107185.

[24] Wu W, Lai Y, Zhang M, Xu X, Pei W, *et al*. Experimental study and micromechanics-based general constitutive theoretical framework for cold-region rocks under triaxial compression. *Int. J. Plast.* 2025, 195:104499.

[25] Mo J, Zeng L, Zhou X, Zhou W, Lin W, *et al*. Triaxial compressive behavior and failure criterion of PVA fiber-reinforced rubberized concrete. *J. Build. Eng.* 2026, 124:116013.

[26] Wu Y, Liu C, Bai G, Liu H, Meng Y, *et al*. 3D printed concrete with recycled sand: pore structures and triaxial compression properties. *Cem. Concr. Compos.* 2023, 139:105048.

[27] Wang G, Lu D, Zhou X, Wu Y, Du X, *et al.* A stress-path-independent damage variable for concrete under multiaxial stress conditions. *Int. J. Solids Struct.* 2020, 206:59–74.

[28] Li L, Zhang B, Joseph P, Zhang X, Zhang L. An investigation of macro- and micro-structural properties of concrete with ceramic waste powder as a sustainable cement substitute. *J. Build. Eng.* 2025, 116:114634.

[29] Ma Z, Guo J, Wu W, Liang C, Hou S, *et al.* Synergistic use of recycled concrete powder, sea sand and seawater for novel ultra-high-ductility cementitious composite: micro-characteristics and mechanical behavior. *J. Build. Eng.* 2025, 113:114103.

[30] Thakur MM, Pattisapu BS, Li W, Meng M, Hurley RC. Material heterogeneity-driven fracture propagation in concrete. *Int. J. Mech. Sci.* 2026, 313:111300.